Fourth International Symposium on Marine Propulsors
smp'15, Austin, Texas, USA, June 2015

Experimental Study on Wake Fields of a Horizontal Axis Tidal Stream Turbine Model in Various Loading Conditions

Jeonghwa Seo[1], SeongTaek Park[1], Seung-Jae Lee[2], Shin Hyung Rhee[1,2]

[1]Department of Naval Architecture and Ocean Engineering, Seoul National University, Seoul, Korea
[2] Research Institute of Marine Systems Engineering, Seoul National University, Seoul, Korea

ABSTRACT

The present study aims to investigate wake characteristics of a horizontal axis tidal stream turbine in various tip-speed-ratio (TSR) conditions. Wake fields were measured by a towed underwater stereoscopic particle image velocimetry (SPIV) system. The scale ratio of the turbine model was 1/20 and the Reynolds numbers based on 0.4R chord length ranged from 53,000 to 63,000. The turbine was rotating in constant revolution rate of 240 rpm, while advance speeds of the turbine model was varied to achieve various TSR conditions. After the global force measurements, four TSRs were chosen for the wake field measurements: the heavy loading, highest efficiency, intermediate loading, and rapid decrease of the performance. In the highest efficiency condition, we observed spatially homogeneous wake and strong tip vortex. Phase-averaged wake fields were also measured to investigate the vortical wake structure.

Keywords

Horizontal axis tidal stream turbine, Model test, Stereoscopic particle image velocimetry

1 INTRODUCTION

Tidal turbines have the potential to play an important role in renewable energy. Because water has higher energy density than air, tidal turbines are more efficient and produce more energy than wind turbines. Hence tidal turbines are typically smaller in size as compared to wind turbines. Also, tides are reliable and easy to predict the direction and magnitude. There are two types of tidal turbines: horizontal axis tidal stream turbine (HATST) and vertical axis tidal stream turbine (VATST). VATSTs are theoretically less efficient than HATSTs; a number of studies have focused more on HATSTs.

Blade element momentum theory (BEMT) is the simplest method to predict the performance of a HATST. Each blade is divided into several spanwise sections, and the lift and drag forces for each two-dimensional section are computed and integrated along the entire length of the blade. Batten et al. (2006) applied BEMT to design HATSTs with two different blade sections; NACA 63-215 and NACA 63-815. The energy conversion performance and possibility of cavitation were compared and analyzed. Batten et al. (2008) validated BEMT by comparing computed results with experimental results of Bahaj et al. (2007).

Although BEMT produces reliable results with short computation time, a limitation is that it cannot handle three-dimensional (3D) effects inherently, for example, tip vortices and radial flows. To capture viscous 3D flow effects, Computational Fluid Dynamics (CFD) methods have been introduced. Faudot and Dahlhaug (2011) performed CFD analysis and compared it with experiments. Lee et al. (2012) developed two computational procedures for estimating the energy conversion performance of a HATST. In the study, BEMT and CFD results showed good agreement and it was applied to the design of a full scale turbine. They suggested the improved design for a HATST, which has raked tip to suppress cavitation.

Experimental approaches have been also used to study the energy conversion through HATSTs. Test procedures, facility, and conditions for tidal turbines were developed based on those of marine propellers first. Bahaj et al. (2007) tested an 800 mm diameter model in a cavitation tunnel and a towing tank. Torque and thrust characteristics were investigated with variations of immersion depth, TSR, hub pitch angle, and yaw angle, as well as the cavitation characteristics in high TSR conditions. Luznik et al. (2013) investigated effects of surface waves on performance of a HATST in a towing tank, and it was found that surface wave limits lower range of working TSRs. Similar experimental study was carried out by Galloway et al. (2014) and in addition they considered effects of yawing angles.

Arrays of tidal stream turbines, like a wind farm, are typically placed in locations of strong tidal flow. In the case of multiple HATSTs, the wake of upstream turbine might affect downstream turbines and wake interference can induce

problems of noise, vibration, and efficiency reduction. Therefore study on turbine wakes, as well as the performance of a single HATST, has been required.

For predicting energy conversion performance of HATST array, Turnock et al. (2011) developed a method combined with BEMT and Reynolds-averaged Navier Stokes equations (RANSE) computation. Lateral spacing of turbines was varied to find out optimal locations. Churchfield et al. (2013) performed large eddy simulation (LES) to compute flow field around two parallel turbines. In the results, wake interactions between two turbines were investigated.

Since turbine wake includes periodic velocity fluctuations, experimental techniques to measure instantaneous flow velocity have been required. Wang et al. (2007) conducted model tests in a cavitation tunnel to observe cavitation and measured wake fields using a laser Doppler anemometry. In the model test design, TSR range included low TSR conditions with stall on the turbine blades. Wake field characteristics were analyzed in terms of the cavitation noise. Chamorro et al. (2013) measured 3D wake fields of a miniature three-bladed HATST by a 3D particle image velocimtery (PIV) system. Although the test was performed in low Reynolds number conditions because of the miniature model size, wake characteristics such as wake development, trajectory of tip vortices, and turbulent structure could be identified well.

Myers and Bahaj (2010) investigated wake characteristics of mesh disk rotor simulators using an acoustic Doppler velocimetry (ADV) system. Wake retardation and turbulence kinetic energy (TKE) were investigated in various conditions: different thrust coefficients, submersion depths, downstream distances, and seabed roughness. Test results provided basic information for arranging a turbine farm although tests were carried out with simplified disk model instead of a turbine model.

In the previous studies, flow field measurements were conducted with small-scale models in low Reynolds number condition; thus experimental results have limitations in predicting performance and wake structures at full scale. Since turbine wake and performance depends on the Reynolds number, a test model in towing tanks or cavitation tunnels should be as large as possible.

In this paper, energy extraction efficiency of a HATST model was measured via a series of towing tank tests. Turbine wakes were obtained with a towed underwater stereoscopic particle image velocimetry (SPIV) system. Time-mean and phase-averaged wake fields were presented. Flow characteristics of wake behind the turbine were analyzed.

2 EXPERIMENTAL SETUP AND METHOD

2.1 Test Model

A 1/20 scale model of a 100kW-class HATST was used in this study. Its full scale turbine was used in CFD analysis of Lee et al. (2012) and the specific design is described there. The turbine model consisted of three blades with NACA 63-418 cross section. The turbine model radius, R, was 200 *mm*, and the turbine hub radius was $0.15R$. Although a circular cross section is frequently used for wind turbines, the 2:1 ellipse was adopted as the hub fitting between the blade and hub, i.e., $0.15 < r/R < 0.3$, in the present study. Table 1 describes the pitch angle distribution along the radius. Figure 1 shows the design of the test model.

Table 1: Distribution of pitch angle

r/R	Pitch angle (°)
0.3	16.98
0.35	14.59
0.4	12.66
0.45	11.07
0.5	9.75
0.55	8.64
0.6	7.69
0.65	6.87
0.7	6.15
0.75	5.5
0.8	4.91
0.85	4.33
0.9	3.74
0.95	3.02
1	2.5

Figure 1: Test model.

2.2 Test Facility

Experiments were carried out in Seoul National University towing tank. Figure 2 shows a schematic diagram of the towing tank. Its length, width, and depth were 110 *m*, 8 *m*, and 3.5 *m*, respectively.

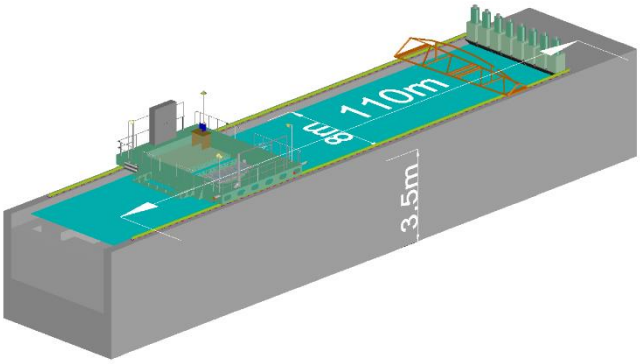

Figure 2: Schematic diagram of the towing tank and carriage

The propeller open water (POW) dynamometer for measuring torque and thrust and towed underwater SPIV system were towed by a towing carriage during measurements. Its maximum speed was 5.0 *m/s* and speed control range was under 0.5% of the input speed. To avoid free-surface effects, the turbine axis was set 500 *mm* under the calm water surface. A minimum distance from blade tip to the calm water surface was 1.5*R*.

A Cartesian coordinate system was used in the study. The positive *x*-axis was in the streamwise direction, the positive *y*-axis was toward the starboard side, and the positive *z*-axis was in vertically upwind direction. The origin was located at the center of the turbine hub.

2.3 Thrust and Torque Measurement System

In the present study, a dynamometer for POW tests was used to rotate the turbine model in a constant revolution rate, 4.0 revolutions per second (*rps*). Torque and thrust on the driving shaft were measured with full-bridge strain gauges. Maximum measurable thrust and torque of the POW dynamometer were 100 *N* and 5 *Nm*, respectively. Signals from strain gauges were measured by MGC plus data acquisition system (manufactured by Hottinger Baldwin Messtechnik GmbH in Darmstadt, Germany.)

According to the principle of HATST performance, power acting on the circumferential and axial direction is non-dimensionalized by the kinetic energy flux of the fluid through the turbine disk area; thus, there are two loading coefficients: the power (torque) coefficient and the thrust coefficient. The power coefficient indicates effective work for rotating the turbine shaft, thus it is the most important parameter in HATST design. The power coefficient, C_p, can be defined as

$$C_p = \frac{Q\omega}{0.5\pi\rho V_A^3 R^2}, \quad (1)$$

where Q is the measured torque on the turbine shaft, ω is the angular velocity of the turbine, ρ is the density of water, and V_A is the advance speed of the model. The thrust coefficient implies axial loading on the turbine. It is not related to energy conversion efficiency, but implies drag on the turbine system only. The thrust coefficient, C_t, was defined as

$$C_t = \frac{T}{0.5\pi\rho V_A^2 R^2}, \quad (2)$$

where T is the measured negative thrust.

2.4. Test Conditions

Revolution rate of the model turbine was fixed at 4 rps, and the advance speed was changed in various TSR conditions. The turbine revolution rate was set based on the maximum measurable thrust and torque range of the dynamometer. TSR was defined as follows.

$$TSR = \frac{R\omega}{V_A} \quad (3)$$

In the test conditions, representative chord-based Reynolds number at 0.4*R* ranged from 53,000 to 63,000. Thrust and torque measurements were carried out first to assess the energy extracting efficiency of the turbine model. Then, four TSR conditions were chosen for wake measurements. Table 2 shows the test conditions for SPIV measurement.

Table 2: Test conditions for SPIV measurement

TSR	Revolution rate (*RPS*)	V_A (*m/s*)	C_P	Characteristics in performance
3.0	4	1.676	0.108	Rapidly reduced efficiency
3.3	4	1.523	0.205	Intermediately increasing efficiency
3.5	4	1.436	0.276	Highest efficiency
4.0	4	1.257	0.253	Decreasing efficiency

2.5. SPIV System

A towed underwater SPIV system which consisted of two underwater cameras with a resolution of five megapixels and 200 *mJ* Nd:YAG dual head pulse laser was used to measure the turbine wake. The system can acquire particle image pairs with a repetition rate of 7.2 *Hz*. In the test, total 150 pairs of particle images were captured during one carriage run. Polyamide particle with the average diameter of 28 μm was used as the tracer particle. For one day of tests, one kilogram of tracer particle was spread into the towing tank.

Figure 3 shows the arrangement of optical components of the SPIV system and the test model. In experiments, flow fields in *y*-z plane which is perpendicular to the turbine axis were measured. Using a camera lens with the focal length of 50 *mm*, the size of the field of view was 250 *mm*× 200 *mm*. Measurement planes located from 0.27*R* to 1.27*R* in axial direction. The distance between measurement planes was 0.1 R for test conditions with TSR of 3.0, 3.3, and 4.0. In the highest power coefficient case with TSR of 3.5, the distance between measurement planes was 0.05*R*.

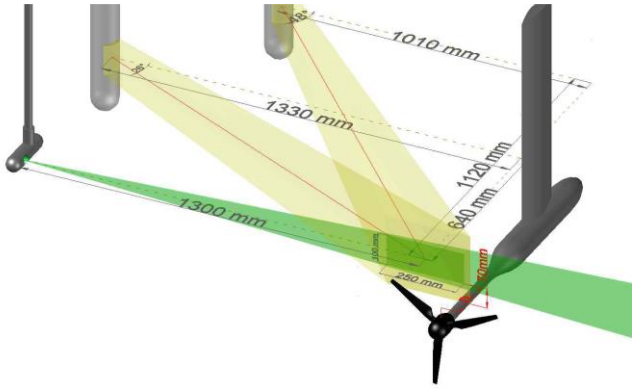

Figure 3: Arrangement of the SPIV system and the test model.

Recorded particle image pairs were analyzed by DaVis V8.1, provided by LaVision GmbH (Gottingen, Germany), to compute instantaneous velocity fields. Distortion of particle images was corrected first and 2D cross correlation on the corrected images was applied. A multi-pass cross correlation method was used to find out precise representative displacement of interrogation windows. Cross correlation was iteratively executed three times. The size of the initial interrogation window was 64×64 pixels without overlap and the size of the second and third interrogation windows was 32×32 pixels with 50% overlap. One representative velocity vector occupied an area of 1.3 *mm*× 1.3 *mm* on the physical measurement plane.

3 RESULTS AND DISCUSSION

3.1 Thrust and Power Coefficient

Figure 4 shows the power coefficient and thrust coefficient obtained in various TSR conditions. When TSR was over 3.25, power coefficient increased rapidly. At TSR of 3.5, power coefficient recorded the largest value, 0.278, as the effective work onto the turbine shaft became maximum. In high TSR cases, power coefficient decreased gradually, but the thrust coefficient increased slightly. Total loading on the turbine at TSR of 4.0, therefore, was similar to that at TSR of 3.5.

As used in BEMT methods, turbine performance could be analyzed by the angle of attack and force acting on blade sections. Figure 5 shows the distribution of the angle of attack along the radius for four different TSRs. The angle of attack was geometrically derived from pitch angle, angular velocity, and the inflow magnitude. As TSR decreased, the angle of attack increased. Stall might occur at the lowest TSR, as discussed in the study of Wang et al. (2007).

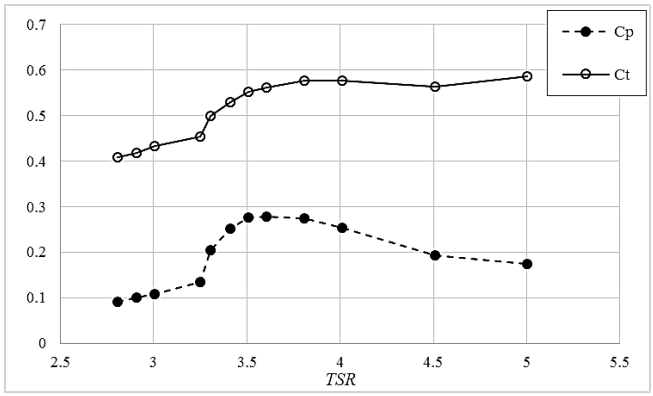

Figure 4: The power and thrust coefficient.

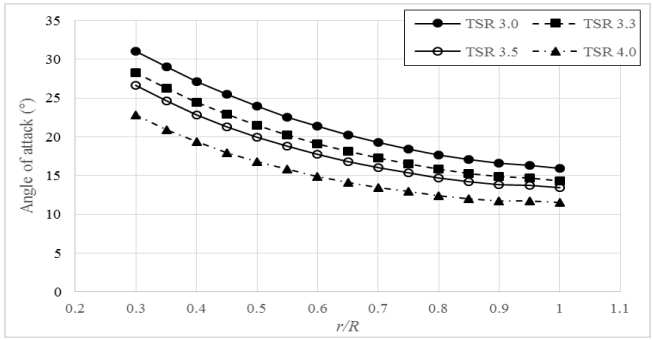

Figure 5: The derived angle of attack onto the blade.

3.2 Time-mean Wake Field

Figure 6 shows the time-mean wake field at TSR of 3.5. The turbine extracted the kinetic energy from the flow, and the wake retarded. The wake shows rotational flow in clockwise direction when looking upstream as the reaction to the rotation of the turbine model.

Velocity distribution along the broken line in Figure 6 was extracted and shown in Figure 7. Circumferential component of velocity was observed near the turbine axis. As shown in Figure 5, the angle of attack onto the turbine blade section near the turbine axis was large, resulting in strong lift force on the blade section. Strong lift accompanied downwash flow developed into the circumferential flow in the 3D turbine wake. Radial flow was observed out of the wake stream, implying expansion of the wake region.

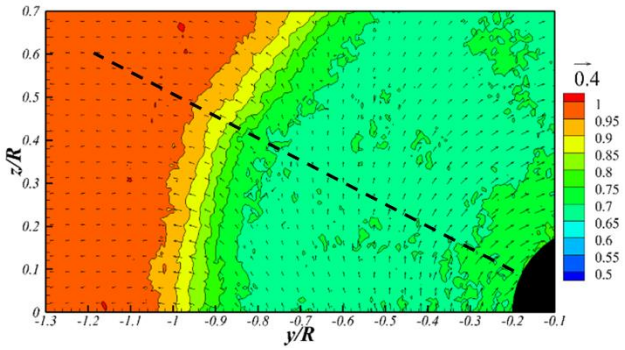

Figure 6: Time-mean u/V_A contours and v/V_A and w/V_A vectors at *x/R* = 0.27and TSR 3.5.

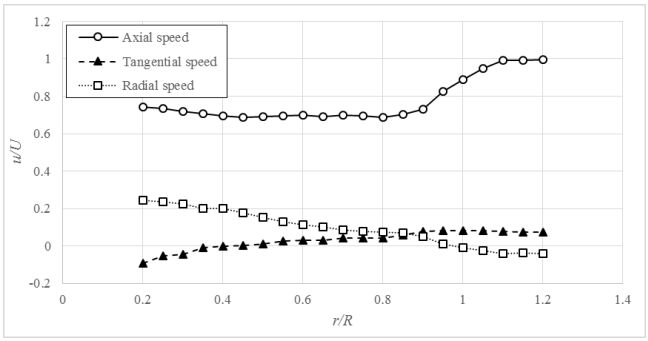

Figure 7: Velocity components at *x/R* = 0.27and TSR of 3.5.

Changes of the axial velocity in different axial locations are shown in Figure 8. The axial velocity retarded downstream as the pressure in the wake recovered. It is opposite to the marine propellers where the wake pressure is high and wake accelerates.

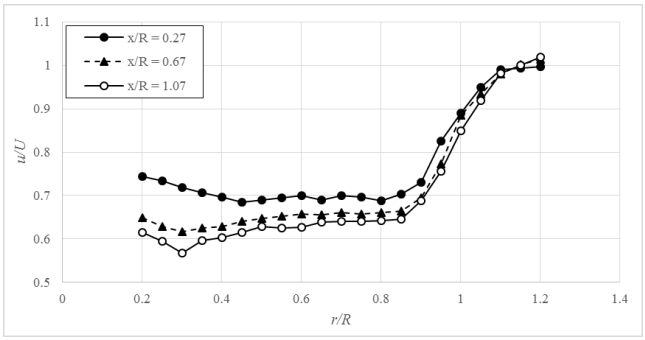

Figure 8: Axial velocity of the wake in different axial locations at TSR of 3.5.

Time-mean wake field at *x/R* = 0.27 were shown in Figure 9. Wake measured at TSR of 3.3, 3.5, and 4.0 shows similar tendency, but the wake at TSR of 3.0 was faster than that at other TSR conditions. The boundary of the wake stream with rapid change of the axial velocity along radial direction was not identified clearly. As shown in Figure 5, the angle of attack onto the blade angle was excessive at low TSR condition and the flow around the blade section could be separated by stall. With stall, energy extraction was seriously disturbed, thus the power coefficient decreased and the wake preserved the kinetic energy.

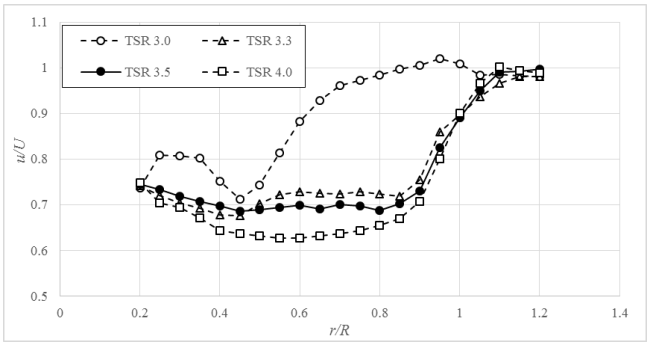

Figure 9: Axial velocity of the wake flow at different TSR conditions.

In the wake measurements, uniformity of wake distribution along the radial direction correlated with energy extracting performance. At TSR of 3.5 with the best performance, axial velocity distribution was uniform along radial direction as each cross section of the turbine blade was in designed angle of attack condition. At TSR of 3.3 and 4.0, the radial distribution of axial speed of wake flow varied with irregular angle of attack onto blade sections, and showed lower efficiency than that in TSR of 3.5.

3.3 Phase-Averaged Wake Field

Phase-averaged wake measurements are shown in Figure 10. Intensive vortex on *y-z* plane was observed and could be identified as tip vortex, except for TSR of 3.0. At the region, the magnitude of the velocity changed rapidly. In the TSR condition, tip vortex with rotating flow did not exist, but there were low speed regions, implying existence of flow separation rather than tip vortex generation. Tip vortices were developed by pressure difference between two sides of the blade. At TSR 3.0, loading and pressure difference on the turbine blade was small due to stall, and tip vortex did not develop.

Figure 11 shows axial vorticity distribution at *x/R* = 0.47. In the flow field measurements, strong tip vortex could be clearly identified at TSR 3.3, 3.5, and 4.0. At the center of vortices, pressure drops and cavitation may occur. As reported in the experimental study by Bahaj et al. (2007), tip vortex cavitation generally exists in high TSR conditions and strong tip vortex observed in the present study also hint

possibility of tip vortex cavitation; thus, operation of HATST at high TSR condition should be avoided, as the tip vortex cavitation may damage other turbines. At TSR of 3.0, vortical flow was not clearly identified due to stall on the blade.

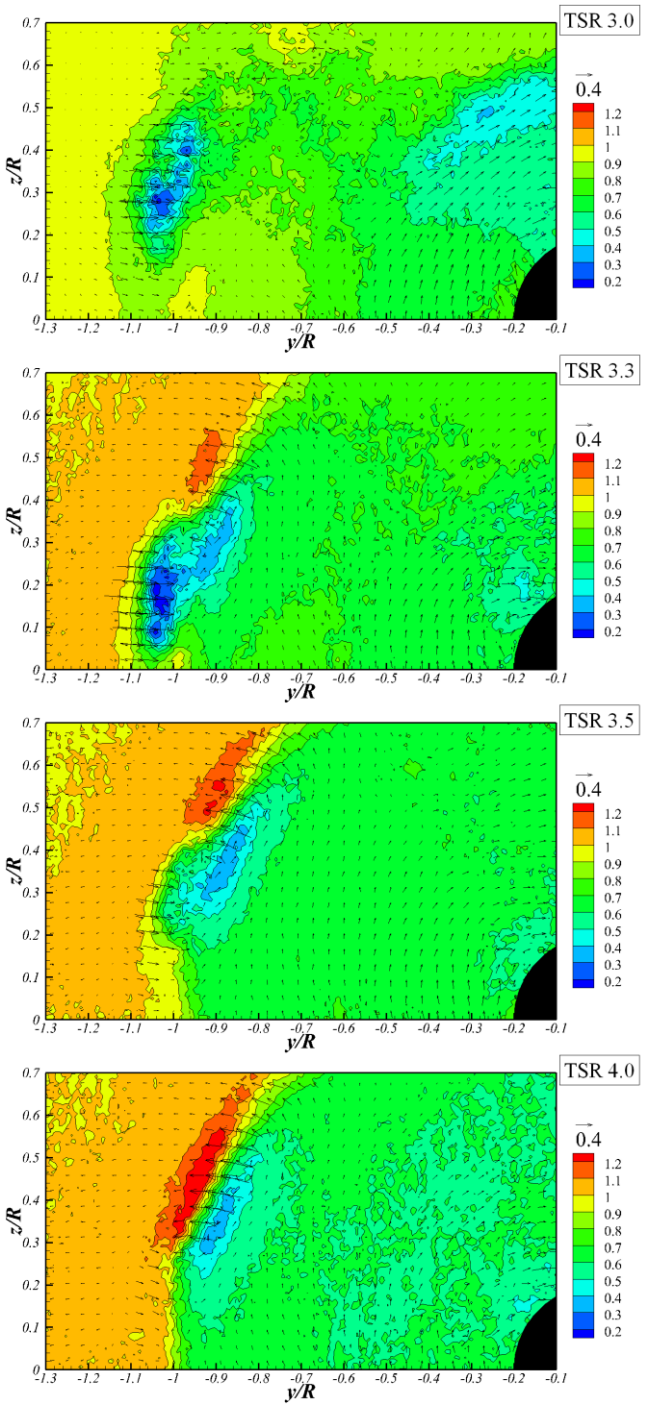

Figure 10: Phase-averaged u/V_A contours and v/V_A and w/V_A vectors at x/R = 0.27.

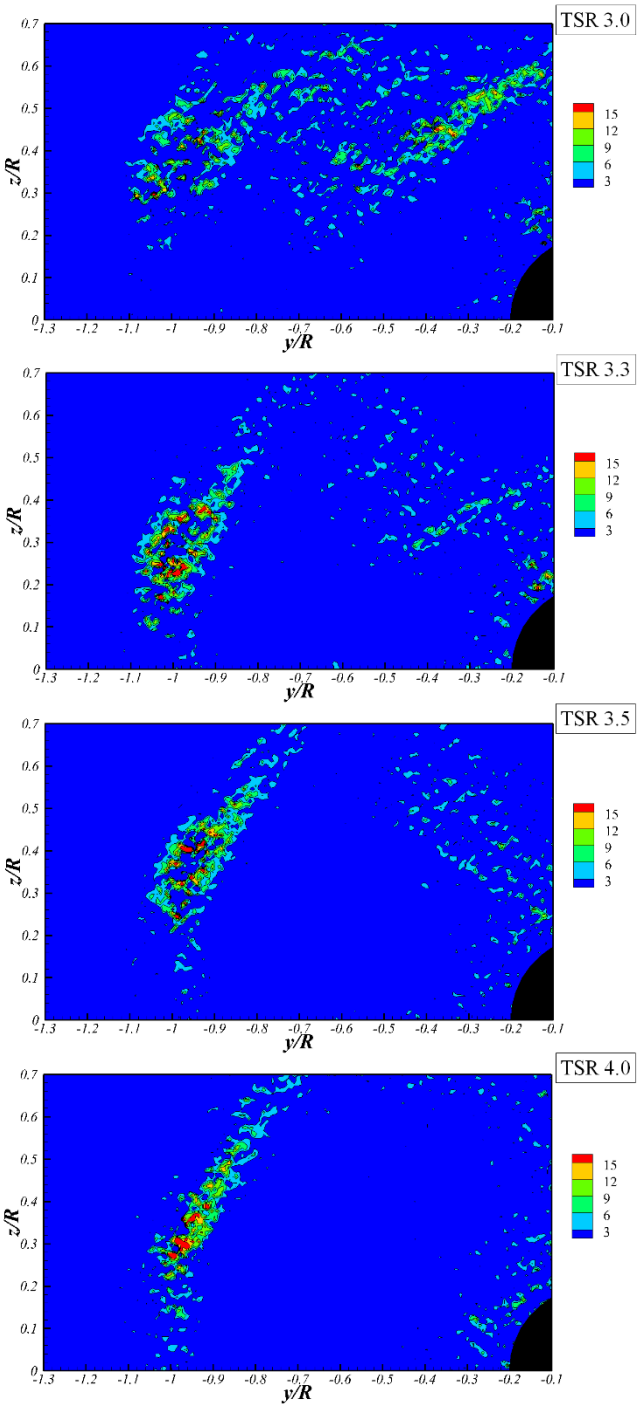

Figure 11: Axial vorticity ($\zeta_x R/V_A$) contours at x/R = 0.27.

4 CONCLUSIONS

Global force and wake fields of a HATST model in various TSR conditions were measured in a towing tank. Measured thrust and torque were analyzed to identify the energy extraction efficiency of the turbine in different TSR conditions. The maximum power coefficient was found at the designed TSR condition and it decreased rapidly at lower

TSR conditions owing to increasing angle of attack onto the blade sections.

Measured flow fields were analyzed in terms of time-mean and phase-averaged velocity field. In the case with the highest power coefficient, axial velocity was uniform along radial direction. In the downstream, axial flow retarded due to recovery of pressure in the wake stream. Kinetic energy of the wake stream decreased as loading on the turbine blade increased. For application of turbine farm, excessively retarded wake should be avoided, thus operation of HATSTs in the low TSR condition without stall in large angle of attack was recommended. It can be achieved by pitch control system of HATST.

Tip vortex was identified in the phase-averaged flow field, except the case with stall. In the tip vortex region, strong axial vortex and high gradient of axial velocity were observed. It preserved in downstream locations.

With the flow field measurements, characteristics of the wake field of HATST could be identified and investigated. Experimental technique and results in the present study can be extended to tests of multiple HATST arrangements.

ACKNOWLEDGMENTS

Support for this research was provided by the National Research Foundation of Korea (Grant No. 2013R1A1A2012597 and 2011-0020563) and Multi-Phenomena CFD Research Center (Grant No. 20090093103) funded by the Ministry of Education, Science and Technology of the Korea government.

REFERENCES

Bahaj, A. S., Molland, A. F., Chaplin, J. R., and Batten, W. M. J. (2007), "Power and Thrust Measurements of Marine Current Turbines under Various Hydrodynamic Flow Conditions in a Cavitation Tunnel and a Towing Tank," Renewable Energy, 32(3), 407-426.

Batten, W. M. J., Bahaj, A. S., Molland, A. F., and Chaplin, J. R. (2006), "Hydrodynamics of Marine Current Turbines," Renewable Energy, 31(2), 249-256.

Batten, W. M. J., Bahaj, A. S., Molland, A. F., and Chaplin, J. R. (2008), "The Prediction of the Hydrodynamic Performance of Marine Current Turbines," Renewable Energy, 33(5), 1085-1096.

Chamorro, L. P., Troolin, D. R., Lee, S. J., Arndt, R. E. A., and Sotiropoulos, F. (2013), "Three-dimensional Visualization in the Wake of a Miniature Axial-flow Hydrokinetic Turbine," Experiments in Fluids, 54(2), 1-12.

Churchfield, M. J., Li, Y., and Moriarty, P. J. (2013),"A Large-eddy Simulation Study of Wake Propagation and Power Production in an Array of Tidal-current Turbines,"Philosophical Transactions of the Royal Society A: Mathematical, Physical and Engineering Sciences, 371(1985).

Faudot, C. and Dahlhaug, O. G. (2011), "Tidal Turbine Blades: Design and Dynamic Loads Estimation Using CFD and Blade Element Momentum Theory," Proc. Of 30th International Conference on Ocean, Offshore and Arctic Engineering, Rotterdam, the Netherlands.

Galloway, P. W., Myers, L. E., and Bahaj, A.S. (2014), "Quantifying Wave and Yaw Effects on a Scale Tidal Stream Turbine," Renewable Energy, 63, 297-307.

Lee, J. H., Park, S., Kim, D. H., Rhee, S. H., and Kim, M.-C. (2012), "Computational Methods for Performance of Horizontal Axis Tidal Stream Turbines," Applied Energy, 98, 512-523.

Luznik, L., Flack, K. A., Lust, E. E., and Taylor, K. (2013), "The Effect of Surface Waves on the Performance Characteristics of a Model Tidal Turbine," Renewable Energy, 58, 108-114.

Myers, L.E. and Bahaj, A.S. (2010), "Experimental Analysis of the Flow Field around Horizontal Axis Tidal Turbines by Use of Scale Mesh Disk Rotor Simulators," Ocean Engineering, 37(2), 218-227.

Turnock, S.R., Phillips, A. B., Banks, J., and Nicholls-Lee, R. (2011), "Modelling Tidal Current Turbine Wakes Using a Coupled RANS-BEMT Approach as a Tool for Analysing Power capture of Arrays of Turbines," Ocean Engineering, 38(11-12), 1300-1307.

Wang, D., Atlar, M., and Sampson, R. (2007), "An Experimental Investigation on Cavitation, Noise, and Slipstream Characteristics of Ocean stream Turbines," Proceedings of the Institution of Mechanical Engineers, Part A: Journal of Power and Energy, 221(2), 219-231.

DISCUSSION

Question from Mehmet Atlar

The authors would like consult or include another slipstream flow investigations of tidal turbines using LDA of the three components of the slipstream velocities by Wang D. et al. (2006 and 2009) in 2006 MAREC symposium in London and 2009 Journal of power technology. Thank you.

Authors' Closure

Thank you for your recommendation. Unfortunately, the authors could not find the original resources of the referred papers; instead we included an experimental study by the same research group in the introduction section. With the

valuable research in cavitation tunnel, we can discuss the physics around the turbine blade with the stall and cavitation.

Question from Dmitry Poukratov

I understand the tidal flow in reality is non-uniform. Are any connections going to be introduced to take in account the flow non-uniformity on the wake?

Authors' Closure

Thank you for your question and your suggestion. As you pointed out, there is inflow variations in direction and magnitude in practical operation conditions, such as disturbance from the seabed. Taking into account the inflow and loading changes in reality, it is needed to conduct performance prediction in various TSRs. Currently we are working on off-design conditions of the turbine, including the non-uniform flow and seabed effects, as they are hard to be achieved by towing tank tests. .